PROCEEDINGS OF SCIENCE

Gamma-ray emission from young supernova remnants in dense environments

R. Brose,[a,*] **I. Sushch**[b,c] **and J. Mackey**[a]

[a] *Dublin Institute for Advanced Studies, Astronomy & Astrophysics Section, DIAS Dunsink Observatory, Dublin D15 XR2R, Ireland*

[b] *Centre for Space Research, North-West University, 2520 Potchefstroom, South Africa*

[c] *Astronomical Observatory of Ivan Franko National University of Lviv, Kyryla i Methodia 8, 79005 Lviv, Ukraine*

E-mail: broserob@cp.dias.ie

Supernova remnants are known to accelerate cosmic rays on account of their non-thermal emission in different wavebands. However, evidence that SNRs do indeed accelerate cosmic rays to PeV-energies is elusive. The idea emerged that PeV-energies might only be reached during the very initial stages of a remnant's evolution. Unfortunately, early gamma-ray emission is strongly attenuated by $\gamma\gamma$-absorption. Here, we investigate how the interaction of SNR-shocks with dense structures in the medium around luminous blue variable (LBV) and Red Supergiant (RSG) stars can boost the gamma-ray emission later.

We use the time-dependent acceleration code RATPaC to study the acceleration of cosmic rays in supernovae expanding into dense environments around massive stars. We investigated typical parameters of the circumstellar medium (CSM) in the freely expanding winds and added dense structures that arise from episodes of highly-enhanced mass-loss of LBVs and photoionized shells around RSGs.

We find that the interactions with the dense structures happens typically after a few months for LBV progenitors and a few years for RSG progenitors. During the interaction stage, the $\gamma\gamma$-absorption by photons emitted from the Supernova's photosphere became negligible. The gamma-ray luminosity of the interacting SNRs can surpass the internal/unabsorbed peak-luminosity that arises shortly after the explosion. Further, the change of the shock-speed during the shock-shell interaction boosts the achievable maximum energy beyond a PeV for LBVs, where early interactions yield higher peak-energies. The later is indicative of potentially efficient acceleration of particles in Fast Blue Optical Transients that have similar CSM-structures to cases considered here.

38th International Cosmic Ray Conference (ICRC2023)
26 July - 3 August, 2023
Nagoya, Japan

*Speaker

PoS(ICRC2023)855

1. Introduction

Supernova remnants (SNRs) stand out as strong contenders for being the origin of Galactic Cosmic Rays (CRs) [2, 7]. However, establishing their capability to accelerate CRs up to the required 3 PeV remains elusive. The limits imposed by observations suggest that the highest attainable energy is around 100 TeV, and even youthful SNRs like Tycho and Casiopeia A exhibit lower cutoff energies despite their young age [1].

Bell et al. [5] propose that the density gradient of CRs is adequately significant only during the initial two decades of SNR evolution, driving turbulence to scales that matter (for PeV CR production) through the non-resonant streaming instability. Alongside the gradients originating from the compact shock extension, environments with high particle densities facilitate the ascent to PeV energies [11, 19].

A notable advantage of supernovae exploding within a dense circumstellar medium (CSM) is the enhancement of γ-ray emissions due to p-p interactions. Nevertheless, interactions between the emitted γ-ray photons and photons emitted by the supernova photosphere attenuate the γ-ray flux, particularly in the initial days following the explosion [11, 12].

In this study, we build upon a previous investigation where we demonstrated that even exceptionally dense CSMs cannot guarantee PeV energy acceleration [10]. Here, we examine a CSM characterized not by a uniform composition but by dense shells with which the shock interacts during the initial post-explosion years.

2. Basic equations and assumptions

In this section, we provide a concise overview of the numerical techniques employed in this research. The approaches described in this segment closely resemble those utilized in previous works involving the **R**adiation **A**cceleration **T**ransport **Pa**rallel **C**ode (RATPaC) [10, and references therin].

Here, we outline the fundamental presumptions that underlie our numerical strategy for addressing the Diffusive Shock Acceleration (DSA) quandary. Our approach encompasses a kinetic portrayal of CRs coupled with a thermal leakage injection model, a comprehensive time-dependent treatment of magnetic turbulence, and an incorporation of PLUTO-based hydrodynamics calculations.

2.1 Circumstellar magnetic field

We posit that the hydrodynamic evolution of the Supernova Remnant (SNR) is not significantly influenced by the dynamic presence of the magnetic field. Within and in the vicinity of the SNR, two distinct components contribute to the magnetic field: a macroscopic field, induced by the progenitor's stellar wind, and a turbulent component that results from self-amplification due to the streaming behavior of CRs. The computation of the aggregate magnetic field strength is conducted as follows:

$$B_{\rm tot} = \sqrt{B_0^2 + B_{\rm Turb}^2}\,, \tag{1}$$

where B_0 is the large-scale magnetic field and $B_{\rm Turb}$ the turbulent component (see section 2.3 for details).

Concerning the large-scale field, we use the induction equation by considering a frozen-in field that is conveyed alongside the hydrodynamic flow [25].

To streamline our model, we have omitted the initial zone and adopted the assumption of a magnetic field within the wind, one that adheres to the following pattern:

$$B(r) = B_* \frac{R_*}{r} \,. \tag{2}$$

We absorb all the uncertainties of the surface magnetic-field into the variables B_* and R_*. We assumed for both progenitor stars a fixed product of $B_*(R_*/R_\odot) = 1000\,\mathrm{G}$.

2.2 Cosmic rays

We employ a kinetic methodology to simulate the acceleration of CRs within the framework of the test-particle approximation. We have taken precautions to ensure that the parameters we selected result in a CR pressure that remains under 10% of the shock's ram pressure. The transport equation, which evolves over time, for the differential number density of CRs N [23], is expressed as follows:

$$\frac{\partial N}{\partial t} = \nabla(D_r \nabla N - \mathbf{u}N) - \frac{\partial}{\partial p}\left((N\dot{p}) - \frac{\nabla\cdot\mathbf{u}}{3}Np\right) + Q \,, \tag{3}$$

where D_r denotes the spatial diffusion coefficient, $\mathbf{u}$ the advective velocity, $\dot{p}$ energy losses and Q the source of thermal particles.

The solution to Equation (3) is computed within a reference frame that moves along with the shock, employing the *FiPy*-library [15]. The outer boundary of the grid spans multiple tens of shock radii upstream, facilitating the inclusion of all accelerated particles within the simulation domain.

2.2.1 Injection

We introduce a constant portion of particles from the thermal reservoir as CRs in line with the thermal leakage injection model [8, 18]. The injection efficiency η_i is defined as

$$\eta_i = \frac{4}{3\sqrt{\pi}}(\sigma - 1)\psi^3 e^{-\psi^2} \,. \tag{4}$$

The shock compression-ratio is denoted by σ, and the multiple of the thermal momentum, at which we inject particles by ψ. We use a value of $\psi = 4.2$ and consider a uniform injection efficiency across the entire shock surface.

2.3 Magnetic turbulence

In parallel to the transport equation for CRs, we solve a transport equation for the magnetic turbulence spectrum, assuming Alfvén waves only, and thus calculate the diffusion coefficient self consistently [9]. In this case, the diffusion coefficient varies strongly in space and time and is

coupled to the spectral energy-density per unit logarithmic bandwidth, E_w. The evolution of E_w is described by

$$\frac{\partial E_w}{\partial t} + \nabla \cdot (\mathbf{u} E_w) + k \frac{\partial}{\partial k} \left(k^2 D_k \frac{\partial}{\partial k} \frac{E_w}{k^3} \right) = \\ = 2(\Gamma_g - \Gamma_d) E_w \, . \tag{5}$$

Here, $\mathbf{u}$ denotes the advection velocity, k the wavenumber, D_k the diffusion coefficient in wavenumber space, and Γ_g and Γ_d the growth and damping terms, respectively [9].

The diffusion coefficient of CRs is coupled to E_w by

$$D_r = \frac{4v}{3\pi} r_g \frac{U_m}{E_w} \, , \tag{6}$$

where U_m denotes the energy density of the large-scale magnetic field, v is the particle velocity, and r_g the gyro-radius of the particle.

As initial condition, we used a turbulence spectrum derived from the diffusion coefficient, as suggested by Galactic propagation modeling [26],

$$D_0 = 10^{28} \left(\frac{pc}{10\,\mathrm{GeV}} \right)^{1/3} \left(\frac{B_0}{3\,\mu\mathrm{G}} \right)^{-1/3} \, . \tag{7}$$

However, the initial diffusion coefficient is reduced by a factor of ten on account of numerical constraints.

We use a growth-rate based on the resonant streaming instability [3, 23],

$$\Gamma_g = A \cdot \frac{v_\mathrm{A} p^2 v}{3 E_\mathrm{w}} \left| \frac{\partial N}{\partial r} \right| \, , \tag{8}$$

where v_A is the Alfvén velocity. We incorporated a linear scaling factor denoted as A, in order to artificially augment the amplification process. For the purposes of this study, we set $A = 10$, mirroring the heightened amplification attributed to the non-resonant streaming instability [4, 17].

Cascading balances the growth of magnetic turbulence and consequently, the level of the magnetic field. This phenomenon is elucidated as a diffusion process within the wavenumber space, with the diffusion coefficient being defined by [22, 28]. This phenomenological treatment will result in a Kolmogorov-like spectrum, if cascading is dominant.

2.4 Hydrodynamics

The progression of a SNR devoid of CR feedback can be elucidated using conventional gas-dynamical equations.

$$\frac{\partial}{\partial t} \begin{pmatrix} \rho \\ \mathbf{m} \\ E \end{pmatrix} + \nabla \begin{pmatrix} \rho \mathbf{v} \\ \mathbf{m}\mathbf{v} + P\mathbf{I} \\ (E+P)\mathbf{v} \end{pmatrix}^T = \begin{pmatrix} 0 \\ 0 \\ 0 \end{pmatrix} \tag{9}$$

$$\frac{\rho \mathbf{v}^2}{2} + \frac{P}{\gamma - 1} = E, \tag{10}$$

Table 1: Parameters for the progenitor stars winds and initial remnant sizes [6, 13, 14]. Columns 2-3 give the mass-loss rate (2) and wind velocity (3) (assumed constant) for each of the 3 cases, and columns 4-6 give the initial radius of the SN ejecta at the start of the simulation (4), the total ejecta mass of the SN (5) and the parameter n determining the radial dependence of the ejecta (6) (see text for details).

Model	$\dot{M}\,[M_\odot/\mathrm{yr}]$	V_w [km/s]	R_ej [cm]	$M_\mathrm{ej}\,[M_\odot]$	$M_\mathrm{shell}\,[M_\odot]$	R_shell [mpc]
LBV	10^{-4}	100	$1.2 \cdot 10^{14}$	10	2	0.001-0.061
RSG light	$8.3 \cdot 10^{-5}$	15	$6 \cdot 10^{13}$	3	0.58	0.049
RSG heavy	$8.3 \cdot 10^{-5}$	15	$6 \cdot 10^{13}$	3	4.41	0.03

where ρ is the density of the thermal gas, $\mathbf{v}$ the plasma velocity, $\mathbf{m} = \mathbf{v}\rho$ the momentum density, P the thermal pressure of the gas and E the total energy density of the ideal gas with $\gamma = 5/3$. Under the premise of spherical symmetry in a one-dimensional context, the set of equations is solved employing the PLUTO code [20]. It is important to acknowledge that radiative losses will exert a significant influence on the initial phases of the remnant's development, particularly in the scenario of a highly dense circumstellar medium (CSM). Nevertheless, photons face challenges in escaping easily, necessitating the utilization of an alternate equation of state to precisely depict areas far downstream of the forward shock [21].

2.4.1 Initial conditions for stellar wind and supernova

The initial conditions for simulations can be written as functions of the ejecta-mass M_ej and the explosion energy E_ej. We used the SN parameters given in Table 1 and an explosion energy of $E_\mathrm{ej} = 10^{51}$ erg for the different progenitor stars.

The stellar wind properties ($\dot{M}$ and V_w) in Table 1 determine the CSM density of the smooth wind that the SN ejecta interact with. The smooth wind leads to the development of a $\rho(r) \propto 1/r$ density profile. Additionally, we placed dense shells with a Gaussian shape in the wind, that originate either from past episodes of enhanced mass-loss for LBVs or by the interaction of the dense wind with the ambient photon fields (RSGs). The shell densities are shown in the same table.

3. Results

3.1 Maximum particle energies

At each time step, the simulated proton spectrum is fitted with a power-law with exponential cut-off in momentum space. The time evolution of the fitting parameter, $E_\mathrm{max} = \sqrt{(p_\mathrm{max}c)^2 + (m_0c^2)^2}$, for our four different configurations is shown in Figure 1.

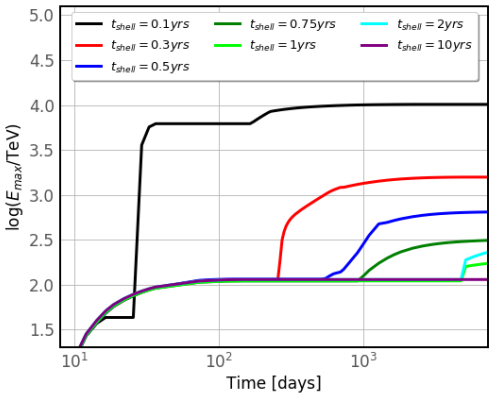

Figure 1: Maximum energy of protons for a LBV progenitors. The times in the caption indicate the time when the forward-shock interacts the first time with the dense shell.

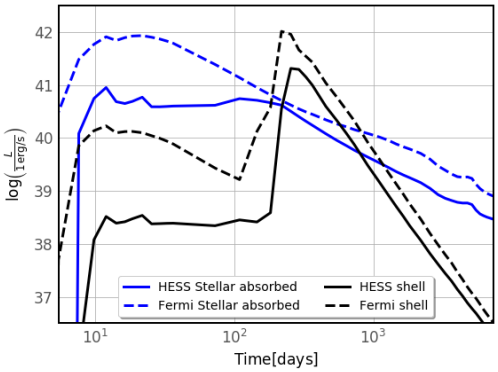

Figure 2: Gamma-ray luminosities in the *Fermi-LAT* energy range (dashed) and *H.E.S.S.* energy range (solid) for smooth winds (blue) [10] and the case of a LBV shock-shell-interaction after 0.3 yrs (black) accounting for $\gamma\gamma$-absorption.

The interactions with the dense shells introduces additional structures in evolution of the maximum energy for LBV-progenitors, if the interaction takes place in the first two years after the explosion. In all this cases, the maximum energy is enhanced after the shock passed through the shell, however, the strength of the increase in the maximum energy depends on the time of the interaction. In general the earlier the interaction, the higher $E_{\rm max}$ rises. For an early interaction at ≈ 0.1 yrs, $E_{\rm max}$ surpasses 10 PeV.

In our earlier work, it became evident, that the non-linear instability is only undergoing 3-5 growth-cycles and thus not able to reach its saturation level [10], a finding suporter by the work of [16]. However, in our case, $E_{\rm max}$ was thus limited to sub-PeV energies, where many other other works found higher energies. In case of the interaction with the dense shells, $E_{\rm max}$ gets now boosted by two mechanisms:

1. The shock-shell interaction slows down the shock considerably and suddenly enhances the precursor-scale $D(E)/v_{\rm sh}$. The time available to grow turbulence in the precursor is enhanced. After the shock passed the shell, the precursor scale is decreased again and the shock runs through a medium with a now pre-amplified field, boosting $E_{\rm max}$. The strength of this effect still depends on the available current, which tends to be higher for an early interaction.

2. The collision of the forward-shock with a dense shell creates reflected shocks, that can be re-reflected at the contact discontinuity an catch-up with the forward-shock from behind. This interaction enhances the forward shocks speed and slightly boosts $E_{\rm max}$, as seen around a few 100 days for the LBV scenario with the earliest interaction-time. Similar effects have been described earlier for reflected shocks that get created due the the interaction of the SNR-shock with the termination-shocks of the progenitor stars wind-bubble [24].

In case of the RSG-progenitors, the interaction happens after ≈ 5 yrs, too late to significantly boost $E_{\rm max}$. However, there, the shells can have an even higher mass then for the LBV-progenitors, thus boosting their gamma-ray luminosity.

3.2 Gamma-ray emission

We derived the γ-ray luminosity in the 1-10 TeV (hereafter *H.E.S.S.*) and 1-300 GeV (hereafter *Fermi*) energy bands. Figure 2 illustrates the evolution of the γ-ray luminosity for one of our LBV-models in comparison with our earlier work on smooth winds.

The shock-shell interaction can clearly be seen as peak in the gamma-ray emission after $\approx$ 100 days. Here, the peak-luminosity is clearly higher then the luminosity that is reached in the first weeks after explosion, the time where most IACTs undertake their pointed observations. In fact, the gamma-ray emission is three orders of magnitude higher in the *H.E.S.S.*-band and two orders of magnitude higher in the *Fermi*-band, compared to the early emission, underlining that these shock-shell interactions clearly enhance the detection-prospects of gamma-ray emission from the objects.

Our reference-model from [10] used a unrealistically high mass-loss rate of $10^{-2} M_{\odot}$/yr. Still, the peak luminosity of our shell-interaction model surpasses the luminosity of our reference model by a factor of ≈ 5 in the *H.E.S.S.*-band and reaches the same luminosity in the *Fermi*-band which is less affected by $\gamma\gamma$-absorption. This means, that the detection horizon for these objects is about a factor of 2 greater for instruments observing VHE gamma-rays, and thus roughly 2 Mpc and 6 Mpc for H.E.S.S. and CTA-south respectively.

3.3 Radio emission

We calculated the radio emission based on the electron distribution and the magnetic field, including the self-amplified component. Figure 3 shows the radio luminosity at 8 GHz, including the effects of free-free absorption in the CSM, and the evolution of the radio spectral index.

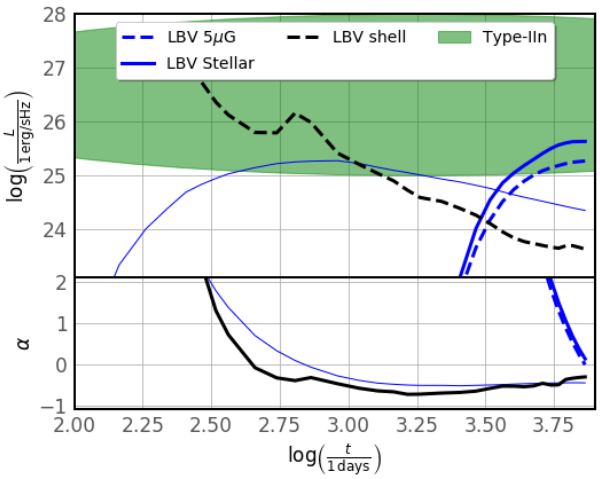

Figure 3: Top panel: Absorbed radio luminosity for a Type-IIn explosions. The dashed, black line is for a shock-shell interaction at 0.3 yrs. Blue lines are models for steady winds with high (thick) moderate (thin) mass-loss rates and an alternative field configuration (dashed). The green area indicates the 1σ uncertainty region for the rise-time and peak radio-luminosity for Type-IIn SN respectively.
Bottom panel: Radio spectral index α of the absorbed radio flux at 5 GHz.

Where our previous work struggled to explain the observed peak-luminosity of the radio-emission either by strong free-free absorption or too low magnetic fields for moderate mass-loss, the shock-shell interaction scenario overcomes both shortcomings. As soon, as the shock has passed the majority of the dense shell, the radio emission can freely escape whereas the interaction itself boosts magnetic field amplification to levels commensurate with the observed radio-flux. The observed peak is now well in agreement with the population study of radio SNe from [6].

Interestingly, the shell-interaction is affecting the radio spectral index by softening it. When absorption became negligible, the radio index is softer then $\alpha = -0.5$ but gradually hardens over

time. The reason is, that during the shell-interaction at each succeeding time, more particles are injected then before. As the acceleration is not instantaneous, this causes a hardening of the spectrum. The effect fades, once the shock has passed the shell and when recently accelerated particles start to dominate. A similar effect of a gradual radio-hardening, starting from a soft spectrum, can be seen in the case of SN1987A [27]. There, the shock interacted with a dense equatorial ring, the sparked a strong brightening in the radio and X-ray emission of the remnant - a situation that is, despite the different geometry, comparable with our simulation-setup.

4. Conclusions

We performed numerical simulations of particle acceleration in very young SNRs expanding in dense circumstellar media featuring dense shells created by the progenitors, solving time-dependent transport equations of CRs and magnetic turbulence in the test-particle limit alongside the standard gas-dynamical equations for CC-SNRs. We derived the CR diffusion coefficient from the spectrum of magnetic turbulence that evolves through driving by the CR-pressure gradient, as well as cascading and wave damping.

The maximum proton energy that we observe in our simulations is exceeding PeV-energies when the shock is interaction prior to ≈ 100 days with a shell of about $2M_{\odot}$. Later interactions still boost $E_{\rm max}$ but not beyond the PeV-frontier.

The peak luminosity in the gamma-ray domain reaches during the shock-shell interaction is well exceeding the initial luminosities of the first weeks after the explosion that are strongly affected by $\gamma\gamma$-absorption. In the VHE-domain, the peak-luminosity during the interaction is about a factor of 5 higher then the luminosity expected from a progenitor with a smooth wind that is about a factor of 100 denser then the case that we consider.

We investigated the radio emission, taking into account the effect of free-free absorption in the ambient medium. We find peak-luminosities consistent with the population average for Type-IIn explosions. The radio spectral index appears soft right after the free-free absorption became negligible and gradually hardens towards the canonical $\alpha = -0.5$.

Acknowledgments

R. Brose acknowledges funding from the Irish Research Council under the Government of Ireland Postdoctoral Fellowship program. I. Sushch acknowledges support by the National Research Foundation of South Africa (Grant Number 132276).

References

[1] Abeysekara A. U., et al., 2020, ApJ, 894, 51

[2] Baade W., Zwicky F., 1934, Proceedings of the National Academy of Science, 20, 259

[3] Bell A. R., 1978, MNRAS, 182, 147

[4] Bell A. R., 2004, MNRAS, 353, 550

[5] Bell A. R., Schure K. M., Reville B., Giacinti G., 2013, MNRAS, 431, 415

[6] Bietenholz M. F., Bartel N., Argo M., Dua R., Ryder S., Soderberg A., 2021, ApJ, 908, 75

[7] Blandford R., Eichler D., 1987, Physics Reports, 154, 1

[8] Blasi P., Gabici S., Vannoni G., 2005, MNRAS, 361, 907

[9] Brose R., Telezhinsky I., Pohl M., 2016, A&A, 593, A20

[10] Brose R., Sushch I., Mackey J., 2022, MNRAS, 516, 492

[11] Cristofari P., Renaud M., Marcowith A., Dwarkadas V. V., Tatischeff V., 2020, MNRAS, 494, 2760

[12] Cristofari P., Marcowith A., Renaud M., Dwarkadas V. V., Tatischeff V., Giacinti G., Peretti E., Sol H., 2022, MNRAS, 511, 3321

[13] Dwarkadas V. V., 2014, MNRAS, 440, 1917

[14] Grassitelli L., Langer N., Mackey J., Gräfener G., Grin N. J., Sander A. A. C., Vink J. S., 2021, A&A, 647, A99

[15] Guyer J. E., Wheeler D., Warren J. A., 2009, Computing in Science and Engineering, 11, 6

[16] Inoue T., Marcowith A., Giacinti G., Jan van Marle A., Nishino S., 2021, ApJ, 922, 7

[17] Lucek S. G., Bell A. R., 2000, MNRAS, 314, 65

[18] Malkov M. A., 1998, Physical Review E, 58, 4911

[19] Marcowith A., Dwarkadas V. V., Renaud M., Tatischeff V., Giacinti G., 2018, MNRAS, 479, 4470

[20] Mignone A., Bodo G., Massaglia S., Matsakos T., Tesileanu O., Zanni C., Ferrari A., 2007, ApJS, 170, 228

[21] Orlando S., et al., 2019, A&A, 622, A73

[22] Schlickeiser R., 2002, Cosmic Ray Astrophysics

[23] Skilling J., 1975, MNRAS, 172, 557

[24] Sushch I., Brose R., Pohl M., Plotko P., Das S., 2022, ApJ, 926, 140

[25] Telezhinsky I., Dwarkadas V. V., Pohl M., 2013, A&A, 552, A102

[26] Trotta R., Jóhannesson G., Moskalenko I. V., Porter T. A., Ruiz de Austri R., Strong A. W., 2011, ApJ, 729, 106

[27] Zanardo G., et al., 2010, ApJ, 710, 1515

[28] Zhou Y., Matthaeus W. H., 1990, Journal of Geophysics Research, 95, 14881